GEOMETRIC VALIDATION OF LOW AND HIGH-RESOLUTION ASAR IMAGERY

David Small[(1)], Betlem Rosich[(2)], Adrian Schubert[(1)], Erich Meier[(1)], Daniel Nüesch[(1)]

[(1)]Remote Sensing Laboratories; University of Zürich
Winterthurerstrasse 190; CH-8057 Zürich; Switzerland
Email: david.small@geo.unizh.ch

[(2)]ESA-ESRIN
Via Galileo Galilei; I-00044 Frascati; Italy
Email: betlem.rosich@esa.int

ABSTRACT

We present issues and solutions concerning the calibration and validation of ENVISAT ASAR image products – both their geometry and radiometry are investigated. Concerning geometric calibration, the slant range products (IMS, APS) offer the best available resolution. We tabulate differences between measured (in image products) and predicted (via geodetic position, precise state vectors, and range and Doppler equations) positions of calibration targets such as transponders and corner reflectors. The differences are interpreted and used to calibrate and validate timing annotation conventions in both the range and azimuth dimensions. For 7 IMS products covering corner reflectors deployed outside Zürich, Switzerland, differences between predictions and measurements were below 3m.

The ENVISAT ASAR modes include single-beam image (IM) and alternating polarisation (AP) modes, as well as wide swath (WS), and global monitoring (GM): ScanSAR modes that cycle through swaths at different incidence angles. The geometry of each mode is validated. We also review validation results for ground range precision products (IMP, APP) and medium resolution products (IMM, APM, WSM) where multiple versions of the polynomial slant/ground range transformation are annotated. We conclude with a demonstration and discussion of the improved retrieval of radiometry that is possible when a well-validated geometry is available.

1. INTRODUCTION

The ENVISAT ASAR sensor can acquire data in a variety of modes: these include (a) the normal imaging mode (**IM**) at a variety of incidence angles, (b) a burst-mode known as alternating polarisation (**AP**) whereby alternate bursts record differing transmit/receive polarisation combinations, (c) wide swath (**WS**), and (d) global monitoring (**GM**). The latter two are ScanSAR modes that cycle through swaths at different incidence angles to allow synthesis of images covering a wider swath (sacrificing resolution). The geometry of ASAR's wave (WV) mode is not treated here.

In addition to the differing *modes*, there are also a variety of *product types* available from the ASAR ground segment. Data acquired in the IM or AP configurations may be processed to the Single-Look-Complex (SLC) level (**IMS** & **APS**), to a high resolution ground range image analogous to ERS PRI products (**IMP** & **APP**), or to strip maps of potentially long azimuth extents at medium resolution: (**IMM** & **APM**). The wide swath (WS) mode images are currently available only in medium resolution ground range format (**WSM**); an SLC product (WSS) is currently under development [2].

Beyond the available acquisition modes and product types, the *orbital state vectors* used during processing (and annotated in all of the above product types) vary in quality from the lowest level (a) flight segment **predicted**, through (b) flight segment **restituted**, (c) DORIS **preliminary**, to the best available (d) DORIS **precise**. For the results presented here, geolocation was performed using precise orbit state vectors (obtained independently of ASAR products) unless otherwise indicated.

2. METHOD

Accurate geometric calibration was performed using products with the highest spatial resolution processed using the most accurate orbital state vectors available. IM and AP single look complex (SLC) products (IMS/APS) were used when the highest precision was required. Previously we characterised the full family of ASAR products and made preliminary comparisons of the absolute location errors of ASAR acquisitions processed using different orbit types [9].

For location error determination, we used the well-surveyed coordinates of relatively easily distinguishable targets such as transponders and corner reflectors to predict their range and azimuth positions in each product, and systematically compared our predictions with the actual location in each product. Large oversampling factors were used in the neighbourhood of the strong targets to measure their actual position at sub-sample resolution. Images of ASAR transponders in the Netherlands and Radarsat transponders in Prince Albert and Fredericton

Proc. of the 2004 Envisat & ERS Symposium, Salzburg, Austria
6-10 September 2004 (ESA SP-572, April 2005)

(Canada), and of corner reflectors outside of Zürich (Switzerland) were used for the study. Image position predictions were made by solving the Doppler and range equations using the target's surveyed coordinates together with the orbit state vectors available and the image timing annotations [6]. Image position measurements were taken with an oversampling factor of fifty. The location of the maximum was chosen as the target's image position *measurement*. That *measurement* was directly compared with the *prediction* to estimate the prediction's accuracy.

The range gate bias (Sampling Window Start Time / SWST bias) was calibrated by measuring range differences between predictions and actual measurements for a set of SLC products processed using precise quality state vectors [9]. All data presented here were processed using the newer (post Dec. 2003) updated SWST bias value.

3. ASAR LOW RESOLUTION VALIDATION

ASAR GM1 products are low resolution (~1 km), far below the acuity of IMM, APM, and WSM products. The resolution gulf is even larger between GM1 products and the high resolution SLC products (IMS & APS). Although the low resolution of GM1 products makes them ill-suited to radar system/timing calibration, a validation of the geometry of the product type is still important to ensure that there are no systematic biases. The multiple slant/ground polynomials that are a feature of IMM, APM, and WSM products are also present in GM1 products, albeit with a generally higher number of updates due to their typical long swaths.

An initial validation of the geometry of ASAR GM1 products was performed by terrain-geocoding using a SRTM model and comparing ASAR radar amplitude with SRTM DEM features. In addition, multiple GM1 products covering the same area acquired from differing incidence angles (also ascending/descending) were terrain-geocoded, overlaid, and inspected for systematic image-to-image shifts.

3.1 Ottawa, Canada

A terrain-geocoded GM1 product of the area surrounding Ottawa, Canada is shown in Fig. 1. It is overlaid on a SRTM DEM with a colour cycle of 500m. Note that no systematic shifts between the DEM colour and ASAR backscatter features are visible (e.g. Ottawa river and valley). For GM1 products processed before May 22, 2004, we found that a single correction factor (available from ESA [1]) must be applied to avoid incorrect azimuth (slow time) scaling. An RGB overlay of three GM1 terrain-geocoded products is shown in Fig. 1(b). Note again the lack of systematic shifts between backscatter features from different dates acquired even from differing satellite tracks and incidence angles.

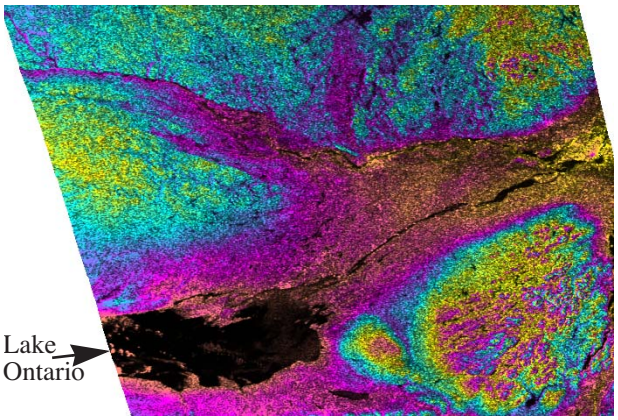

(a)

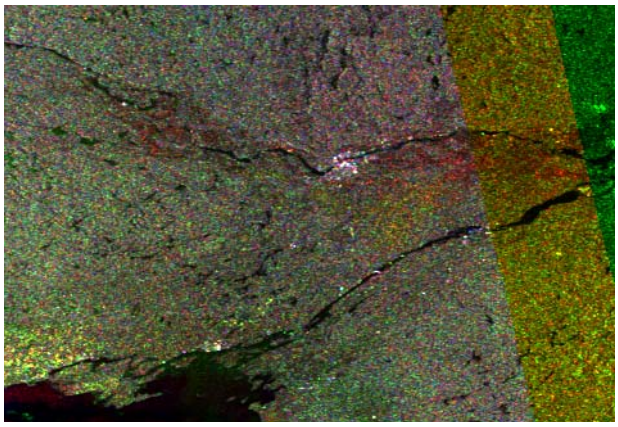

(b)

Fig. 1: Ottawa, Canada terrain-geocoded GM1 products -- (a) ASAR GM1 backscatter amplitude (acquired June 10, 2004) & SRTM 500m height colour cycle; (b) RGB overlay of R=May 25, G=June 10, B=June 13, 2004

3.2 Prince Albert, Canada

A terrain-geocoded GM1 product covering northern Alberta and Saskatchewan in Canada is shown in Fig. 2(a). The GM1 amplitude is juxtaposed with SRTM-height (colour). Again no systematic shift is visible between ASAR backscatter amplitude and SRTM height features (e.g. the Athabasca river and valley running south-north). An overlay of three terrain-geocoded GM1 products (mixture of ascending and descending) for an area south of Lake Athabasca is shown in Fig. 2(b). No systematic shifts are visible between images acquired at differing incidence angles. For example, note the consistently located sharp amplitude gradients at lake edges.

3.3 Eastern Australia

A terrain-geocoded version of a long-swath GM1 product is shown in Fig. 3(a) overlaid on a SRTM DEM with a height cycle of 2000m. The image shows a pass over the eastern part of Australia. Close-ups of the coastal areas are shown in Fig. 3(b) for the north-east and Fig. 3(c) for

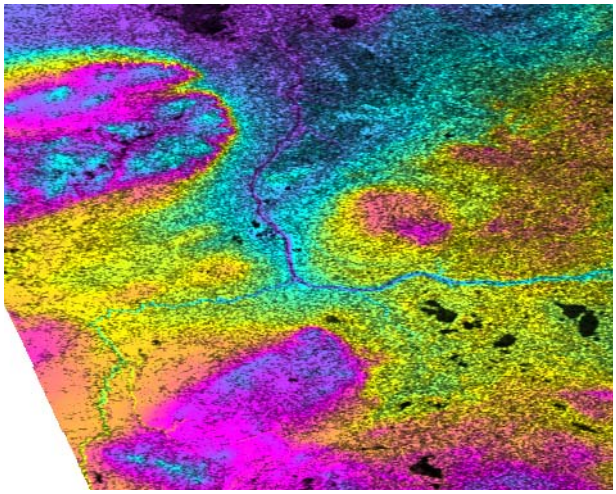

(a)

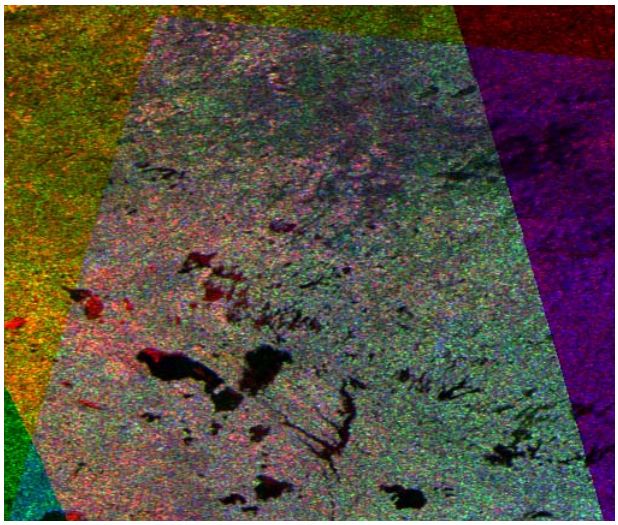

(b)

Fig. 2: Prince Albert, Saskatchewan, Canada terrain-geocoded GM1 products -- (a) ASAR GM1 backscatter amplitude (acquired June 3, 2004) overlaid on SRTM 500m height colour cycle; (b) RGB overlay of terrain-geocoded GM1 images: R=May 28, G=June 3, B=June 2, 2004

the south-east. In these cases, the SRTM height cycle was set to 500m. Note that despite the long swath (and consequently a very large number of slant/ground range polynomial transitions), no systematic shifts are visible between ASAR backscatter and SRTM DEM features - the Whitsunday islands are visible as both amplitude and DEM features in Fig. 3(b), and show excellent co-registration.

4. ASAR HIGH RESOLUTION VALIDATION

In earlier work, we calibrated the ASAR sampling window start time (SWST) bias by comparing predicted and measured **range** positions of transponders and corner reflectors, and later validating [9] the updated value used in operational PF-ASAR processing since Dec. 12, 2003.

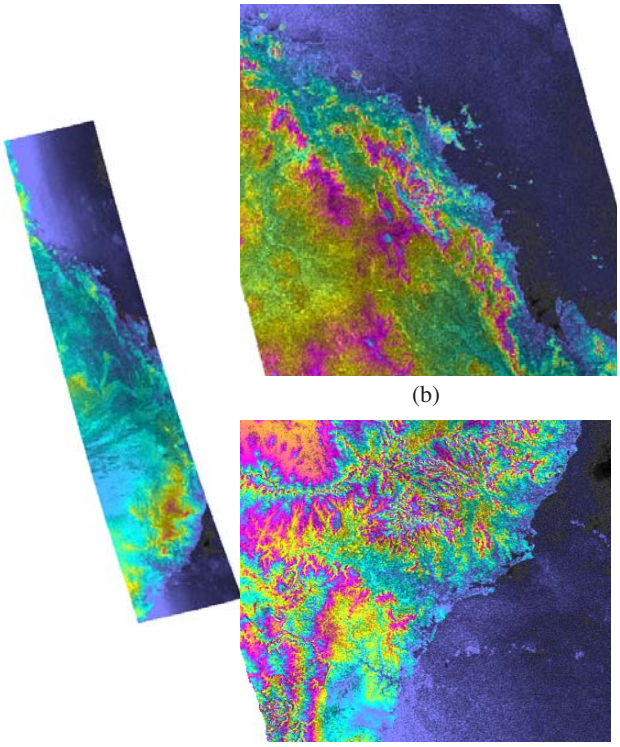

(a) (b) (c)

Fig. 3: Eastern coast of Australia -- terrain-geocoded GM1 products -- (a) ASAR GM1 backscatter amplitude (acquired June 10, 2004) overlaid on SRTM 2km height colour cycle; (b) Whitsunday Islands on NE coast / 500m colour cycle; (c) SE coast / 500m colour cycle

During those validations of IM and AP-mode ASAR imagery, we noted possible residual **azimuth** biases in the prediction, setting the topic aside at the time for later study. We have now undertaken an investigation using image mode SLC data - AP data were not used due to their poor sidelobe ratios [3] and consequent possible contamination of image location measurements. This section summarises the results of the study.

4.1 Azimuth "Bistatic" Bias and Correction

Radar systems generally annotate the signal (raw) data acquired with a time stamp noting the time of reception of each echo. During SAR image focusing, the PF-ASAR processor transforms the image matrix to "Zero-Doppler", shifting each echo *receive* time to *Zero-Doppler* time. However, the time interval between ASAR pulse transmission and echo reception is not compensated. That interval is not Doppler-dependent - its extent depends on the swath imaged (affecting the slant range "fast" time), and can be understood as a "leakage" of range *fast time* into azimuth *slow time*. The issue is strictly an annotation convention, and can be compensated during post-processing (e.g. during geolocation) once its existence is known. Considering an ideal zero-Doppler case, the azi-

muth "bistatic" effect is illustrated in Fig. 4. The relationship between slant range distance r_i and slant range "fast" time t_i is

$$t_i^{Range} = \frac{2 \cdot r_i}{c}, \quad (1)$$

where c is the speed of light. The slant range "fast time" corresponds to the time interval between pulse transmission and echo reception. To translate between time annotation conventions, the receive time is retrieved from Zero-Doppler time by adding half of the slant range "fast time":

$$t_i^{Receive} = t_i^{Zero-Doppler} + \frac{1}{2} t_i^{Range}. \quad (2)$$

Once that correction is applied during geocoding, the location-dependent azimuth time shift may be calculated and compensated. Geolocation and geocoding proceeds otherwise normally. In the following sections, we compare image location predictions done with and without such compensation.

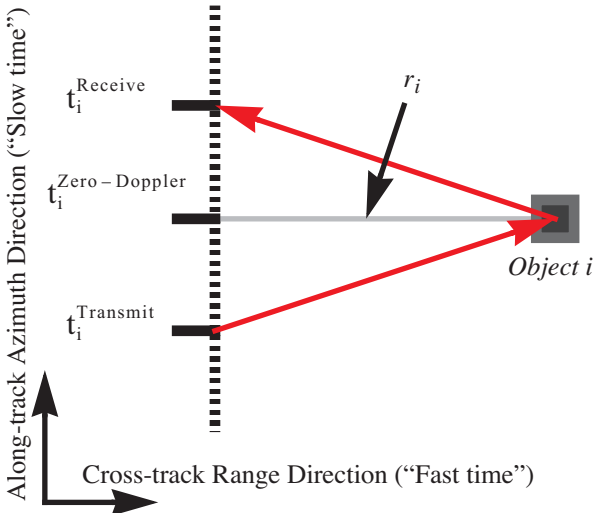

Fig. 4: Azimuth "bistatic" effect in idealised Zero-Doppler case

4.2 Corner Reflectors in Dübendorf, Switzerland

Evaluation of data from corner reflector (CR) campaigns is free of location errors caused by the transponder delay term. In the year 2003, we deployed corner reflectors at at the Dübendorf airport outside of Zürich, Switzerland for geometric calibration and validation. Seven ASAR IM acquisitions are available covering these corner reflectors. We surveyed the corner reflector position before every acquisition with differential GPS. We used each CR's surveyed coordinate together with ENVISAT precise orbit state vector values and the IMS product timing annotations to predict each CR's position in every IMS product. We performed this prediction both *with* and *without* the azimuth bistatic correction described in the previous section.

For the case when bistatic correction was applied, close-ups of the Dübendorf scenes available with surveyed corner reflectors are shown in Fig. 5. The image location predicted on the basis of the CR location, satellite state vectors, and radar timing parameters is marked with a blue cross. Two zoom levels are provided, the native 1×1 single look complex (SLC) image aspect ratio (129×129) in the top row, followed by a 3×3 zoom of the neighbourhood surrounding the prediction location (43×43). The azimuth sample spacing in IMS and APS SLC products is approximately 3-4m. The slant range sample spacing is approximately 8m, and is constant over all incidence angles. A constant slant range resolution translates to varying ground resolutions that are dependent on the incidence angle of the beam used (IS1-IS7). For IMS and APS products, the aspect ratio between nominal slant range and azimuth sample sizes varies between 3 and 6.

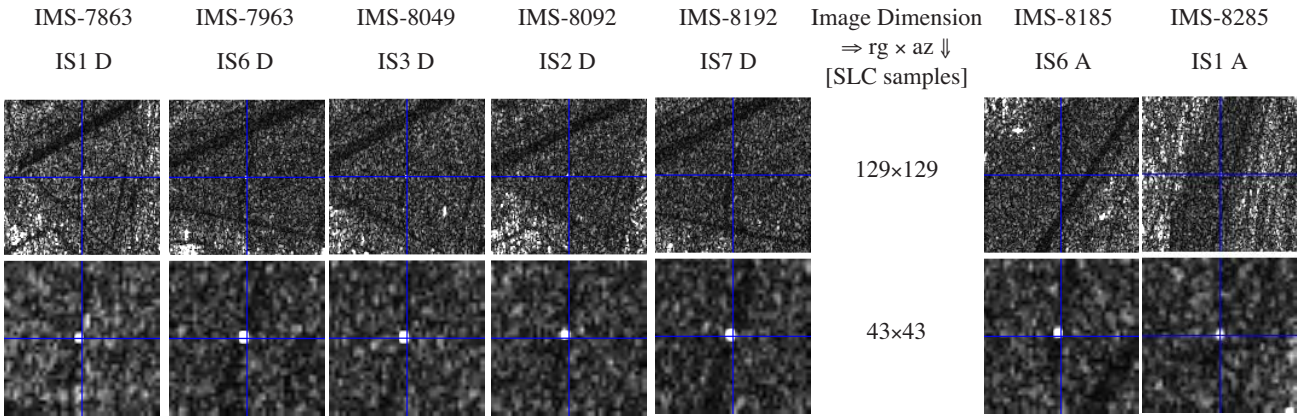

Fig. 5: Dübendorf Corner Reflector Measurements vs. Predictions (restituted orbits) -- Left: Descending (D), Right: Ascending (A)

The ASAR IMS products were ordered through ESA's Payload Data Segment (PDS), and came annotated with restituted state vectors, but were geolocated using precise state vectors obtained independently. Comparisons of the corner reflector position predictions performed *with* vs. *without* the bistatic correction are shown in Fig. 6. Fig. 6(a) shows the differences between prediction and measurement when no bistatic correction was applied; Fig. 6(b) shows the much smaller differences when the correction *was* applied. For (a) & (b) the units are SLC *samples*. On the ground, a single azimuth sample is considerably smaller than a single range sample. Blue crosses are ascending scenes, red/green are descending. Fig. 6(c) and Fig. 6(d) juxtapose the same prediction/measurement differences performed with and without bistatic correction; for (c) & (d), the units are *metres*. The radar's pulse repetition interval (PRI) varies depending on beam, causing a non-linear relationship between the time [samples] and distance [metre] spaces.

The differences between predicted and measured CR positions are shown quantitatively in Table 1 for both azimuth and range directions in SLC *sample* units. Mean deviations of 1.63 m in azimuth and 2.02 m in range are impressively low. Adding the bistatic correction reduces azimuth prediction error by ~20 m. Note that the standard deviation is also reduced, indicating removal of a systematic noise source.

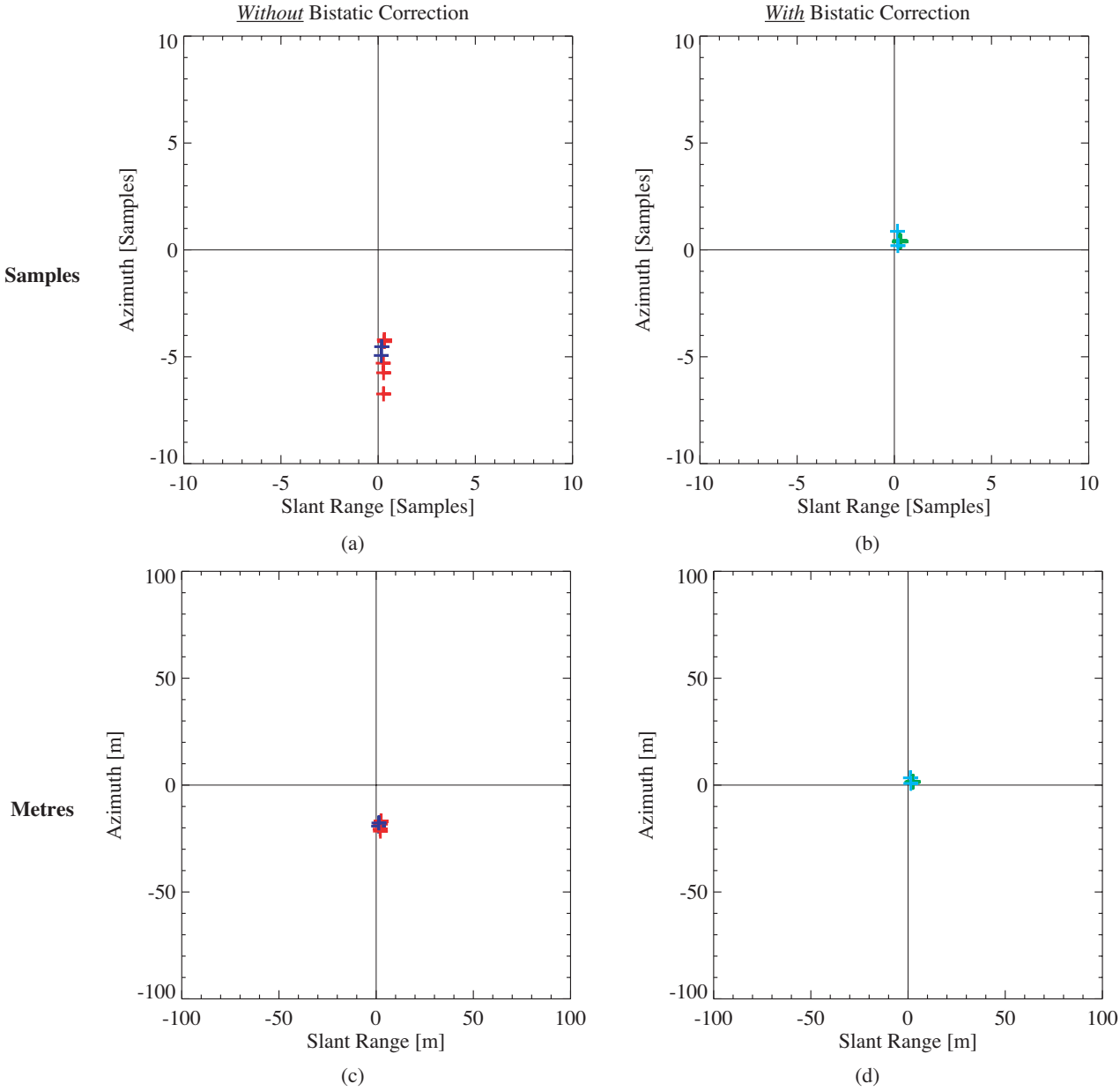

Fig. 6: Differences between predictions and measurements for seven Dübendorf corner reflector positions -- (a) *Without* bistatic correction [Samples], (b) *With* bistatic correction [Samples], (c) *Without* bistatic correction [m], (d) *With* bistatic correction [m]

Orbit	Beam	Prediction - Measurement [*SLC samples*]		Slant Range	SCR
		Azimuth			
		Without Bistatic Correction	*With* Bistatic Correction		
7863	IS1 D	-4.29	0.38	0.33	9.7
7963	IS6 D	-5.30	0.37	0.26	30.3
8049	IS3 D	-5.75	0.44	0.28	21.7
8092	IS2 D	-4.20	0.41	0.32	15.8
8192	IS7 D	-6.74	0.39	0.28	23.0
8185	IS6 A	-4.94	0.87	0.16	12.5
8285	IS1 A	-4.53	0.20	0.18	6.7
Mean and Standard Deviation		-5.11±0.91	0.44±0.21	0.26±0.07	[Samples]
		-18.71±1.83	**1.63**±0.82	**2.02**±0.51	[m]

Table 1: Zürich-Dübendorf Corner Reflectors: Differences between Predictions and Measurements

The signal to clutter ratio (SCR) value listed indicates the strength of the target signal in comparison to the background level, which is measured by averaging the backscatter values within the oversampled area excluding an area immediately surrounding the maximum. The image clutter is usually higher when using beams with relatively steep incidence angles such as IS1 - terrain backscatter generally decreases at shallower incidence angles.

4.3 RADARSAT Transponders in Canada

Eight ASAR IM acquisitions covering the area surrounding the Radarsat transponders deployed in Prince Albert, Saskatchewan and four covering Fredericton, New Brunswick (Canada) were ordered through the PDS. Transponder absolute location errors were then calculated *with* and *without* azimuth "bistatic" corrections. Independently obtained precise orbit state vectors and the improved SWST bias [9] implemented in 2003 were used throughout.

Scatterplots for the **Prince Albert** transponder are shown in Fig. 7 - in Fig. 7(a) *without*, and in Fig. 7(b) *with* bistatic correction applied. Note that the residual errors are larger than seen in the Dübendorf CR results, but still low compared to other spaceborne radars. Comparing Fig. 7(a) to Fig. 7(b), adding the bistatic correction made the azimuth error for ascending vs. descending scenes symmetric about zero, indicating a possible transponder survey inaccuracy. A single scene exhibits an anomalously large range prediction error. Possible causes for the errors are survey and delay term inaccuracies and variations - they will be further investigated.

Scatterplots for the **Fredericton** transponder are shown in Fig. 8 - in Fig. 8(a) *without*, and in Fig. 8(b) *with* bistatic correction applied. The four descending scenes (2 IS2, and 2 IS4) exhibit consistent geolocation errors even for different beams, indicating a possible survey error as the cause. The location error is reduced when bistatic correction is applied.

5. GROUND RANGE PRODUCT VALIDATION

Ground range products require an extra step during geolocation, namely transformation from slant range to ground range - in the case of medium resolution strip map products, the transformations are updated every 10-40 km within a product, requiring special care in selecting and combining the appropriate polynomial transformations.

5.1 Imaging and Alternating Polarisation Modes

ASAR ground range products were previously validated [9] with the best state vectors available. We repeat those validations here with precise state vectors obtained independently. For example IMP and IMM images covering the ASAR transponders in the Netherlands, Fig. 9 illustrates the prediction error. The signal to clutter (SCR) value is also provided for reference. Deviation between prediction and measurement is less than a single sample in both range and azimuth dimensions. For example APP and APM images covering the ASAR transponders in the Netherlands, Fig. 10 illustrates the prediction error. Deviations are again less than a single sample in both range and azimuth dimensions.

5.2 Wide Swath Mode

Multiple ground/slant range polynomials are present in IMM, APM, and WSM products. The location of the ASAR transponders was predicted for two WSM products acquired over the Netherlands, as shown in Fig. 11. The Aalsmeer transponder was outside the acquired area during orbit 9330, and Swifterbant appears not to have responded during either data take. Using precise state vectors, the locations of all visible transponders were predicted to within a single sample accuracy.

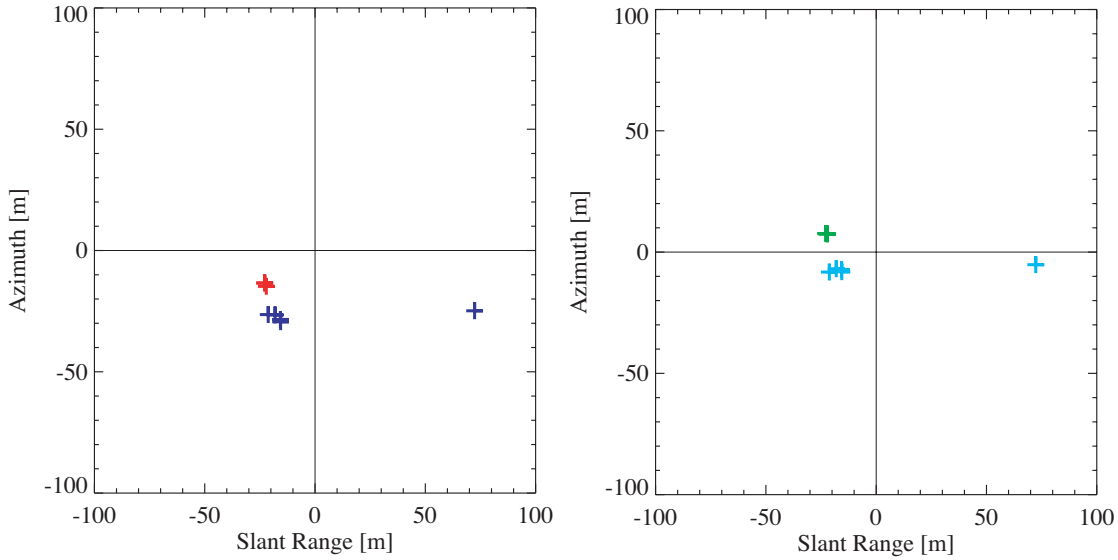

(a) *Without* Bistatic Correction (b) *With* Bistatic Correction

Fig. 7: Differences between Prince Albert transponder position predictions and measurements -- Ascending: 1 IS1, 2 IS3, 2 IS5; Descending: 2 IS4, 1 IS6 -- (a) *Without* bistatic correction [m], (b) *With* bistatic correction [m]

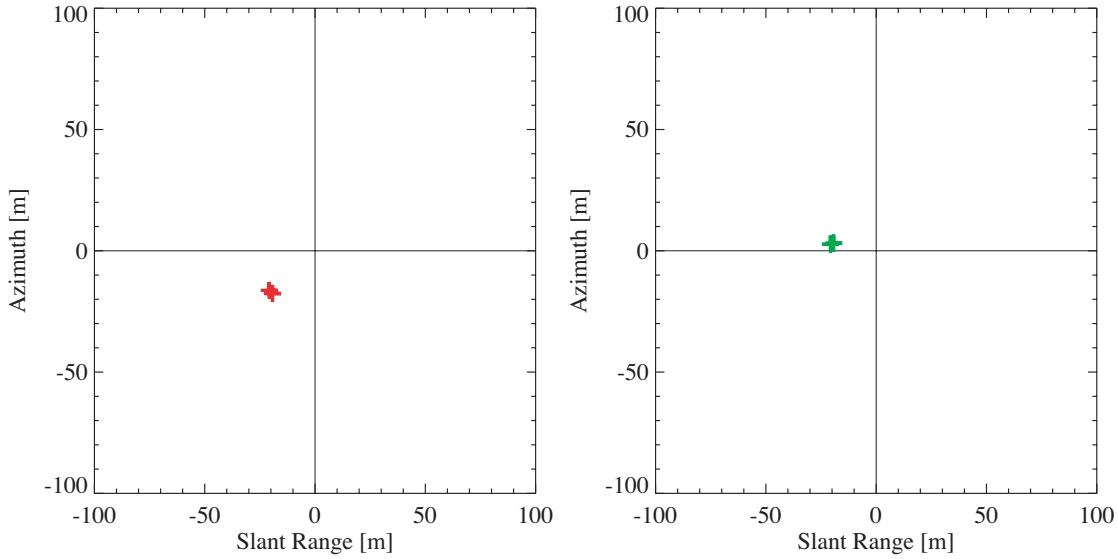

(a) *Without* Bistatic Correction (b) *With* Bistatic Correction

Fig. 8: Differences between Fredericton transponder position predictions and measurements -- Descending: 2 IS2 & 2 IS4 -- (a) *Without* bistatic correction [m], (b) *With* bistatic correction [m]

6. RADIOMETRIC NORMALISATION

One of the benefits of a well-validated geometry is improved radiometric calibration [4], illustrated in Fig. 12. For an ASAR wide swath scene covering most of Switzerland, a conventionally terrain-geocoded (GTC) image is shown in Fig. 12(a). Given a well-validated geometry, an image simulation, as illustrated in Fig. 12(b), may be used to normalise the radar image, removing most topography-induced backscatter influences, and allowing a less encumbered thematic interpretation of the data. The normalised image is labelled radiometrically terrain corrected (RTC) - for the same ASAR wide swath acquisition, an example of this level of processing is shown in Fig. 12(c). If terrain-induced variations in local illuminated area [5] and antenna gain pattern [8] are removed, the remaining non-system-dependent thematic backscatter may be more easily interpreted [10]. Note how cities and high Alpine terrain are more easily separable given the RTC rather than GTC image. These normalisations however require excellent co-registration between the image simulation and input radar image, necessitating highly accurate geometric validation.

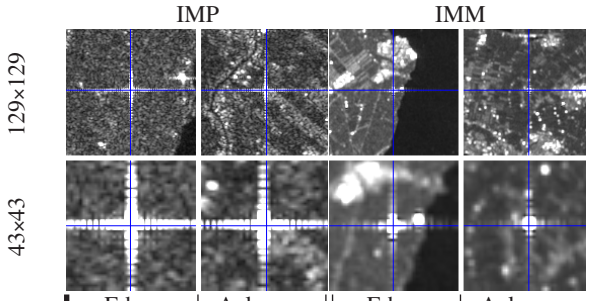

	Edam	Aalsmeer	Edam	Aalsmeer
Az	0.69	0.65	0.08	0.01
Rg	-0.39	0.55	-0.30	-0.14
SCR	264	184	43	30

Fig. 9: Geometry Validation for IMP and IMM Products - Prediction vs. Measurement for ASAR NL-Transponders -- Orbit 7269 IS7 ascending

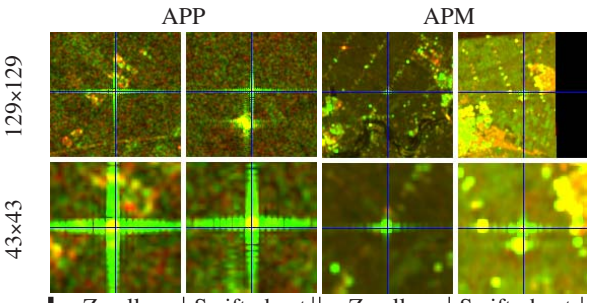

	Zwolle	Swifterbant	Zwolle	Swifterbant
Az	0.49	0.95	0.03	0.09
Rg	0.01	-0.66	0.13	-0.06
SCR	209	130	40	35

Fig. 10: Geometry Validation for APP and APM Products - Prediction vs. Measurement for ASAR NL-Transponders -- Orbit 4542, IS7 descending, HV/HH polarisations

7. CONCLUSIONS

Terrain geocoding has been tested on all ESA ASAR product types (slant and ground range), aside from wave mode and browse products. Image mode (IMS, IMP, IMM), alternating polarisation (APS, APP, APM), wide swath (WSM) and global monitoring (GM1) products have been validated. The standard ellipsoid geocoded products (IMG, APG) were not treated here - earlier results [6] show errors broadly consistent with those of IMS products from the same acquisition. A systematic azimuth "bistatic" bias was discovered, and a method for its compensation described and validated by tabulating corner reflector and transponder absolute location errors.

Since the SWST bias correction was integrated in PDS production on Dec. 12, 2003, range prediction is routinely accurate to the sub-pixel level. Predictability of target image location within ASAR image products is more accurate than experience with other radar sensors. Given state vectors of poorer quality, error sources such as the azimuth "bistatic" effect can become "lost in the noise". In the past, when an absolute location error (ALE) on the order of 100m or a few hundred metres was the goal, low-level error sources could be accepted (or go undetected), but given higher ambitions such as aiming to improve the ALE by an order of magnitude or better, then the list of significant error sources lengthens and additional corrections become necessary. ENVISAT ASAR's accuracy continues to chart new territory.

8. ACKNOWLEDGMENTS

The authors wish to thank the entire crew that helped out during the Dübendorf corner reflector campaign. We would also like to thank ESA for supplying the ASAR data, Prof. Andrea Monti-Guarnieri of POLIMI for suggesting a "bistatic" origin for the azimuth bias, and the Swiss Federal Office of Topography for use of the Swiss *DHM25* digital height model.

9. REFERENCES

[1] ASAR Team, *ASAR Cyclic Report, April - June 2004 Cycles 26, 27, and 28*, ENVI-CLVL-EOPG-TN-04-0009, Issue 1, Revision 0, Aug. 8, 2004. Available at `http://earth.esa.int/pcs/envisat/asar`

[2] Cordey R., Desnos Y.L., Rosich B., *ASAR Wide-Swath Single-Look Complex Products: Processing and Exploitation Potential*, Proc. of Fringe'03 Workshop, ESA-ESRIN, Frascati, Italy, Dec. 1-5, 2003.

[3] Rosich B., Meadows P., Monti-Guarnieri A., *ENVISAT ASAR Product Calibration and Product Quality Status*, Proc. CEOS SAR Workshop, May 27-28, 2004, Ulm, Germany.

[4] Rosich B., Meadows P., *Absolute Calibration of ASAR Level 1 Products Generated with PF-ASAR*, ENVI-CLVL-EOPG-TN-03-0010, Issue 1, Rev. 4, 23 Jan. 2004.

[5] Small D., Biegger S., Nüesch D., *The Topology of SAR Imagery in Rough Topography*, Proc. of EUSAR'2000, Munich, Germany, May 23-25, 2000, pp. 501-504.

[6] Small D., Schubert A., Krüttli U., Meier E., Nüesch D., *Preliminary Validation of ASAR Geometric Accuracy*, Proc. of ENVISAT Validation Workshop, ESA-ESRIN, Frascati, Italy, Dec. 9-13, 2002, ESA SP-531, Aug. 2003.

[7] Small D., Holzner J., Raggam H., Kosmann D., Schubert A., *Geometric Performance of ENVISAT ASAR Products*, Proc. of IGARSS'03, Toulouse, France, July 21-25, 2003, pp. 1121-1123.

[8] Small D., Jehle M., Meier E., Nüesch D., *Radiometric Terrain Correction Incorporating Local Antenna Gain*, Proc. of EUSAR 2004, Ulm, Germany, May 25-27, 2004, pp. 929-932.

[9] Small D., Rosich B., Meier E., Nüesch D., *Geometric Calibration and Validation of ASAR Imagery*, Proc. of CEOS SAR Workshop, Ulm, Germany, May 27-28, 2004.

[10] Small D., Meier E., Nüesch D., *Robust Radiometric Terrain Correction for SAR Image Comparisons*, Proc. of IGARSS'04, Anchorage, Alaska, USA, Sept. 20-24, 2004, pp. 1730-1733.

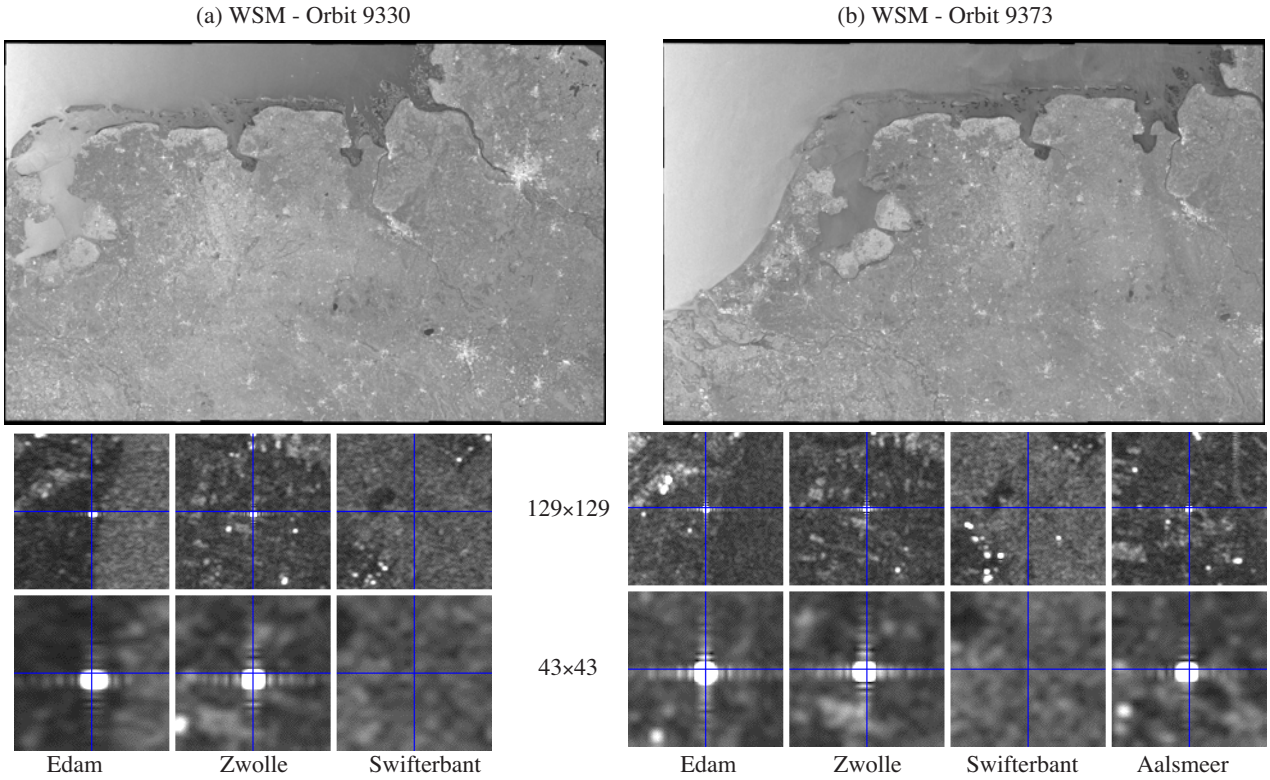

Fig. 11: WSM Transponder Predictions vs. Measurements: The Netherlands - (a) Orbit 9330, (b) Orbit 9373

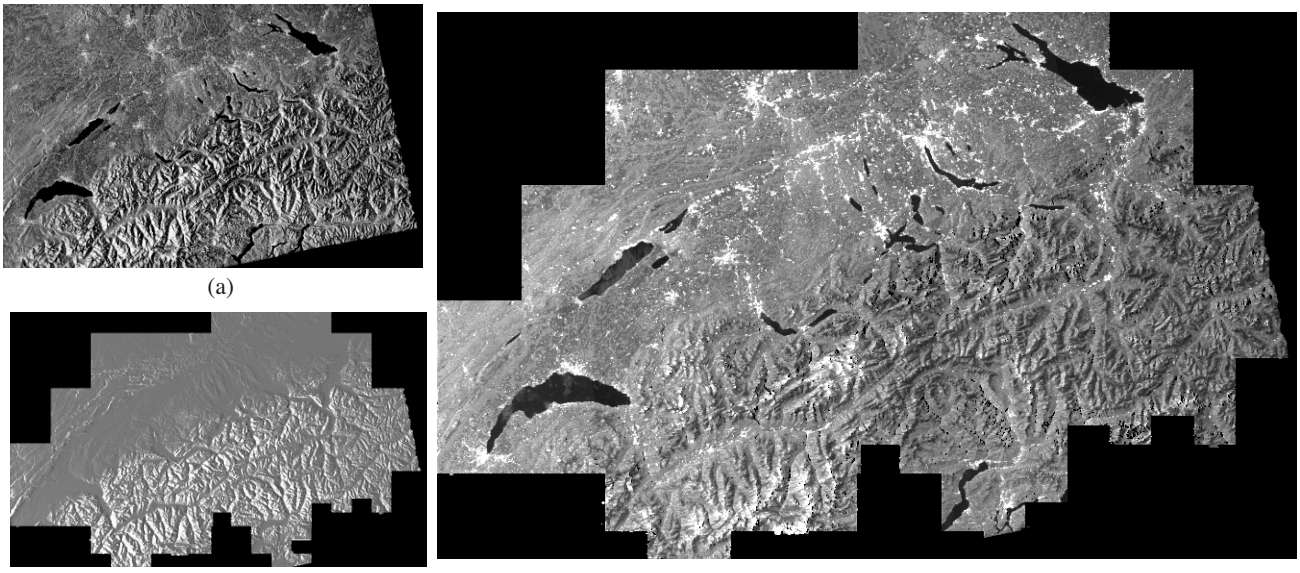

Fig. 12: ASAR Wide Swath over Switzerland: a validated *geometry* enables improved retrieval of *radiometry* -- (a) *Geocoded* Terrain Corrected (GTC), (b) Radiometric Image Simulation (based on *DHM25*), (c) *Radiometrically* Terrain Corrected (RTC)